Materials & Design 228 (2023) 111863

Contents lists available at ScienceDirect

Materials & Design

journal homepage: www.elsevier.com/locate/matdes

Effects of accelerated aging on the appearance and mechanical performance of materials jetting products

Ali Payami Golhin [a,*], Chaman Srivastava [a], Are Strandlie [a], Aditya Suneel Sole [b], Sotirios Grammatikos [a]

[a] ASEMlab – Laboratory of Advanced and Sustainable Engineering Materials, Department of Manufacturing and Civil Engineering, NTNU – Norwegian University of Science and Technology, 2815 Gjøvik, Norway
[b] Department of Computer Science, Norwegian University of Science and Technology, 2815 Gjøvik, Norway

HIGHLIGHTS

- The long-term performance of 3D-printed bilayer polymer structures shows dynamic appearance variation because of the aging effect.
- The changing trend among glass transition temperatures over time is similar and regardless of surface finish.
- Up to 49% more elastic modulus and 4 to 15% higher glass transition temperature due to aging are recorded.
- The maximum variation in mechanical and physicochemical properties is observed following 58 days of accelerated aging.
- Magenta and black photopolymers exhibit the lowest and highest performance during accelerated aging, respectively.

GRAPHICAL ABSTRACT

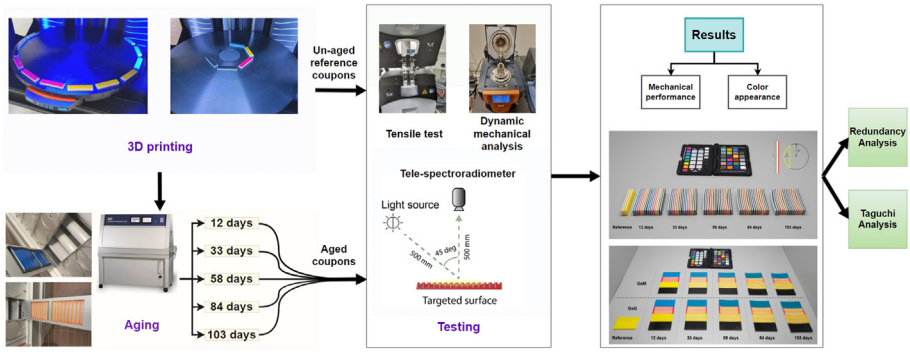

ARTICLE INFO

Article history:
Received 29 January 2023
Revised 14 March 2023
Accepted 22 March 2023
Available online 27 March 2023

Keywords:
Material jetting
Accelerated aging
Dynamic mechanical analysis
Tensile properties

ABSTRACT

As a result of the associated costs and environmental impacts, Material Jetting (MJT) plays a limited role in Additive Manufacturing (AM). Research on the durability and long-term performance of MJT objects by evaluating their appearance is lacking. The objective of this study is to investigate the effect of aging on the color and the physico-mechanical performance of MJT parts. This work examines the influence of production settings on objects subjected to a total of 103days of accelerated aging. The studied Printing Primary Parameters (PPPs) were resin color, build platform position (swath), and finishing configurations. The results indicated the response of the studied PPP according to the aging time was non-linear due to the dynamic appearance response to aging time. VeroBlackPlus and VeroCyan photo resins demonstrated superior color fidelity through aging by a color difference of less than 10. Based on Taguchi and Redundancy Analysis (RDA), mechanical and physicochemical properties varied the most after 58 days

Abbreviations: AM, Additive manufacturing; CCA, Correspondence canonical analysis; CMYK, Cyan, Magenta, Yellow, and Black colors; DCA, Detrended correspondence analysis; DMA, Dynamic mechanical analysis; DoE, Design of Experiments; E, E-modulus (stiffness); E′, Storage modulus; FDM, Fused deposition modeling; GoG, Glossy-on-Glossy finish; GoM, Glossy-on-Matte finish; LOM, Laminated object manufactured; MCDM, Mean color difference from the mean; MJT, Material jetting; PC, Principal component; PCA, Principal component analysis; PPP, Printing primary parameter; RDA, Redundancy analysis; RMSE, Root-mean-square error; rs, Spearman rho; S/N, Signal-to-Noise ratio; SD, Standard deviation; Tan δ peak, Damping; T_g, Glass transition temperature; TSR, Tele-spectroradiometer; σ_s, Tensile strength.

* Corresponding author.
E-mail address: ali.p.golhin@ntnu.no (A.P. Golhin).

https://doi.org/10.1016/j.matdes.2023.111863

Color appearance
Long-term performance

of accelerated aging, with elastic modulus retention up to 149.21% and Glass Transition temperature (T_g) up to 116.6%. This study demonstrates the importance of considering long-term performance during the design process of AM products, depending on the intended application and service conditions.

1. Introduction

Additive Manufacturing (AM) includes methods of creating an object by adding material according to a defined design, layer by layer. AM parts were restricted to the color of the raw material until full-color 3D printing became accessible using polymers. Material Jetting (MJT) technology, including PolyJet® technology, is an AM technique that has revolutionized multi-material 3D printing, employing UV-curable polymer inks. In terms of color reproduction, MJT is one of the main AM categories [1].

The increasing application of polymers in various AM techniques necessitates a thorough understanding of their on-demand long-term performance according to their application. Assessing the long-term performance of parts can be complex and time-consuming. Still, it is common for consumers to associate inferior quality with the visual differences they notice between related items. Color accuracy is critical when printing 3D objects, and the hue of the 3D-printed part should match that of the intended color in the genuine design [2]. Furthermore, the 3D-printed part is expected to be durable and meet quality standards. Developing mass production of 3D-printed items requires accurate reproduction and maintenance of color when using 3D printing for product prototyping. For instance, models used in medical education and surgical planning [3] may benefit from more accurate color representations immediately after printing and over an extended period.

The innovative r-theta rotating build platform concept with a fixed print head is an alternative to conventional XYZ build platforms for 3D printers [4]. The disc-shaped build platform was chosen for numerous reasons, including improved consistency, simplicity in maintenance, and less environmental impact. Although the layering technique and pattern differ from those of other additive manufacturing machines, this necessitates additional thought when assessing design, appearance, and long-term performance. A detailed examination, in particular, exposes some damaged and glued parts in the various assembled models printed on rotational construction platforms. Moreover, the commercial printer creates brittle, stiff components [5].

Although MJT-printed products present an attractive appearance, their long-term performance is crucial because of the high cost and negative environmental effects. Different process Printing Primary Parameters (PPPs) can affect the surface quality of MJT-printed objects, such as varied materials, part design, size, build orientation, surface finish, layer thickness, and environmental factors during use /service [6,7]. Our previous work [4] highlighted the significance of modifying both the placement on the build platform and the model thickness. There is a tradeoff between cheaper and faster 3D printing and accurate color reproduction in the inner area of a rotary build platform. The 3D printing process PPP can also affect the functionality and mechanical performance of both un-aged and aged MJT products. Bass et al. [8] reported the ultimate tensile stress and the elongation of VeroWhitePlus parts increased over time while lighting conditions did not affect material properties significantly. Vu et al. [9] characterized the influence of print build orientations on the fracture strength energy of tri-layer systems comprising an elastomeric material, bridging two glassy-acrylic sections for multi-MJT AM processes. As suggested by Siegfarth et al. [10], MJT can manufacture durable hydraulic actuators for medical robots.

Accelerated aging (weathering test) has been widely employed to study the long-term performance of polymers in laboratory settings. Weathering protocols involve intense aging of specimens for a short duration to replicate long-term natural degradation. The effect on different aging mechanisms should be studied to assess and predict expected long-term performance. Therefore, research based on altering accelerated aging variables over longer exposure time could provide an understanding of degradation in real life [11,12].

Taguchi method of designing experiments can reduce the number of runs and adjust the mean values to a target value [13]. As a result of this approach, it is possible to conduct long-term and costly experiments. Based on the identification of aging degradation mechanisms, the Taguchi method can identify the optimal combination of input variables that will cause the best quality product [14]. Accordingly, the main effects of means and signal-to-noise ratios explain the quality of the manufacturing phase intended for applications, such as surgical planning, tooling, and testing [15].

Understanding the intrinsic correlation between the static and dynamic mechanical response is crucial for comparing mechanical properties, such as stress relaxation, tensile, loss modulus, and creep of materials [16–18]. Due to different layering systems, there is a significant difference between the mechanical performance and appearance of MJT objects and other AM techniques for polymers, such as Fused Deposition Modeling (FDM) [19,20], Laminated Object Manufacturing (LOM) [21], Vat photopolymerization [22] and Selective Laser Sintering (SLS) [23].

Long-term mechanical performance is vital in engineering applications. However, appearance is crucial for several polymer-based products [24], where enhanced aesthetic properties facilitate marketing [1]. Furthermore, performance assessment by mechanical properties is not possible during the service /use /operation of a structure or product [25]. As such, a direct link between appearance and mechanical performance would be ideal for engineering applications. Chen et al. [26] studied the laws of appearance and mechanical behavior in additive manufacturing. However, the concept of appearance in their work was restricted to the morphology and microstructure of AM components, rather than color, gloss, and translucency.

In this study, the mechanical and optical properties of 3D-printed bilayer polymers were examined to assess the performance of the rotary PolyJet method. To the best of our knowledge, this is the first study that relates appearance to durability in materials jetting. The coupons were manufactured by varying three PPPs, namely color, swath selection (position on the build platform), and finishing between the white background and colored layers (finish). The samples were then aged in laboratory conditions following an accelerated aging protocol. The coupons were removed periodically at 12, 33, 58, 84, and 103 days and evaluated in terms of color appearance, as well as physicochemical and mechanical properties. A multivariate analysis using Redundancy Analysis (RDA) was conducted to determine the effects of accelerated aging on appearance and physico-mechanical performance and their interrelationships. The main effect plot studies a link between

color change and mechanical properties. The results investigated the correlation between appearance measurements and mechanical testing to assess the long-term performance of coupons via studying changes in color attributes.

2. Materials and methods

2.1. Materials and manufacturing

The polymeric coupons were manufactured by Stratasys J55 PolyJet 3D printer (Stratasys Ltd., Israel) using VeroCyan (RGD843), VeroBlackPlus (RGD875), VeroYellow (RGD836), VeroMagenta (RGD851), VeroPureWhite (RGD837), and support material (sup710) photo-resins. To designate colors of coupons, "cyan", "magenta", "yellow", and "black" terms have been used throughout this paper as a term for referring to the corresponding primary photo resin materials. The Vero materials from Stratasys include low-viscosity acrylic oligomer, (octahydro-4,7methano-1 H-indenediyl) bis(methylene) diacrylate, 4-(1-oxo-propenyl)-morpholine, and *exo*-1,7,7-trimethylbicyclo hept-2-yl acrylate [27]. The materials datasheet for the Vero photo-resins family shares similar mechanical, thermal, and electrical attributes [28].

The design method follows Pantone-validated color matching procedures and Stratasys best practices for PolyJet, which recommends that printed components have a minimum wall thickness of 1 ± 0.02 mm, creating a white background to ensure optimum color representation [29]. An orthogonal L8 array from Taguchi analysis for three PPPs - color, swath selection, and surface finishing between layers were chosen to examine the influence of 3D printing PPP on the color appearance and mechanical performance as output variables. For this purpose, two configurations of surface finish, including a Glossy colored layer on Glossy (GoG) and Matte (GoM) white substrate, were chosen. The width of the swaths, defined by the area covered by the print heads concerning the radius of the build platform, determines the design positioning (Fig. 1). At least three repetitions in a randomized order were performed for each experimental trial indicated by the orthogonal array. The desirability technique defined a set of three factors that allowed for the simultaneous optimization of all input variables (printing parameters).

To assess the physico-mechanical performance, Dynamic Mechanical Analysis (DMA) and tensile testing were employed on coupons accelerated aged for five aging durations and a total of 103 days of aging (12, 33, 58, 84, and 103 days). For reference, the mechanical property changes of aged coupons were compared to the mechanical properties of un-aged coupons. In this study, color appearance changes were studied using the DMA coupons. In total, 323 polymeric coupons were 3D-printed using eight runs for the five different aging durations, including un-aged reference coupons (0 days). The coupons used for DMA testing were prepared to have a white background of 2 ± 0.02 mm with a colored top layer of 1 ± 0.02 mm. This is due to match the thickness of the colored layer as the tensile testing and having constancy in the colored layer as a PPP. The criteria for each parameter were designed to decrease the constraints imposed by the processing software and 3D printer and the impact of post-processing. Due to the configuration of the build platform, i.e., the rotary disc, the minimum size possible for coupons is considered to reduce the impact of the radial effects on the coupons. Table 1 summarizes the PPP and the Design of Experiments (DoE) levels used for testing.

Table 2 summarizes the types of specimens that were examined according to eight runs of the DoE.

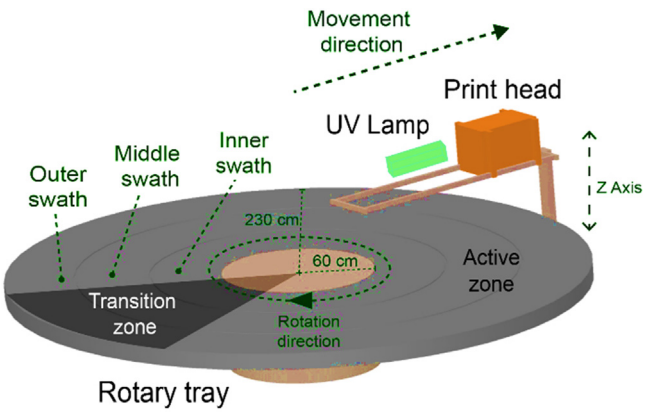

Fig. 1. Illustration of principal components of the build platform in a J55 PolyJet 3D printer.

2.2. Accelerated aging process

To study aging, the manufactured coupons (DMA and tension) were aged in a QUV accelerated aging tester (Q-Lab Corporation, USA) for a total of 103 days. Five different aging intervals were selected to determine the effect of aging over time on appearance and mechanical performance. ASTM G154 standard [30] was used to establish the aging regime resembling accelerated natural weathering. In each weathering cycle, the colored surface of the coupon was exposed to UVA radiation at 340 nm with an intensity of 0.8 W/m^{2}nm for 6 h at 60 °C (Fig. 2). The irradiation was followed by condensation at 40 °C in the dark for 4 h and deionized water spray at 24 °C for 2 h. The coupons were cycled weekly, and two cycles were repeated daily.

2.3. Appearance measurement protocol

Spectral radiance was measured between 380 and 780 nm and under D50 illuminant. Using a CS-2000 (Konica Minolta, Japan) Tele-Spectroradiometer (TSR), the optical resolution was 1 nm, and the physical sample interval was set to 10 nm. The TSR was placed at 50 cm from the target, normal to the surface (Fig. 3 (a)). The measurement field of view was set to 0.2° to prevent inaccuracies caused by targeting areas with dust or stains. A 45°:0° viewing geometry was used for the surface analysis of the 3D-printed specimen following CIE Publication 15.2 [31]. The device was calibrated using the standard Spectralon before each series of measurements. Each measurement was based on average radiance in six locations chosen and evenly distributed around the surface of the DMA coupons immediately after being removed from the aging chamber (Fig. 3 (b)), after wiping the coupons dry with

Table 1
DoE levels and factors.

Run	DoE factor (3D printing parameter)		
	Color [a]	Swath [b]	Finish [c]
1	C	I	GoG
2	C	O	GoM
3	M	I	GoG
4	M	O	GoM
5	Y	I	GoM
6	Y	O	GoG
7	K	I	GoM
8	K	O	GoG

[a] C: Cyan, M: Magenta, Y: Yellow, and K: Black photo resins.
[b] GoG: Glossy-on-Glossy finish, and GoM: Glossy-on-Matte finish.
[c] I: Inner (r-tray less than 105 mm), and O: Outer (169 mm < r-tray < 229 mm) swath.

a paper towel. Errors were reduced by avoiding sites with unusual colors, external particles, and support materials. Measurements of appearance were performed before and after weathering exposure for each sample.

Calculations of colorimetric values were performed in MATLAB R2022a using the computational color science toolbox [32]. A color-matching function, according to ASTM E308-01 [33] was used to calculate CIEXYZ. Thus, tristimulus values were calculated using the CIE 2° color-matching functions under the D50 illuminant. The coordinates for CIEL*a*b* were then determined using CIE1976 and CIEXYZ tristimulus values using Eqs. (1) to (3)

$$L^* = 116(Y/Y_n)^{1/3} - 16 \tag{1}$$

$$a^* = 500\left[(X/X_n)^{1/3} - (Y/Y_n)^{1/3}\right] \tag{2}$$

$$b^* = 200\left[(Y/Y_n)^{1/3} - (Z/Z_n)^{1/3}\right] \tag{3}$$

Table 2
Specimen studied for each of the 8 DoE runs.

	Experiment for each DoE run (Replica × Measurement)			
Aging time (days)	Color appearance	Sagitta	Tensile	DMA
0 – Reference	2 × 3	2 × 1	5 × 1	2 × 1
12	2 × 3	2 × 1	5 × 1	2 × 1
33	2 × 3	2 × 1	5 × 1	2 × 1
58	2 × 3	2 × 1	5 × 1	2 × 1
84	2 × 3	2 × 1	5 × 1	2 × 1
103	2 × 3	2 × 1	5 × 1	2 × 1

where X_n, Y_n, and Z_n stand for the tristimulus values of Spectralon. Using Eqs. (4) and (5), CIEL*C*h* values were determined to calculate the color difference according to CIEDE2000

$$C^* = \sqrt{a^{*2} + b^{*2}} \tag{4}$$

$$h^* = \arctan(b^*/a^*) \tag{5}$$

CIEDE2000 colorimetric difference was calculated between control samples (un-aged) and the same sample after weathering, according to Eq. (6)

$$CIEDE2000 = \sqrt{\left(\frac{\Delta L^*}{k_L S_L}\right)^2 + \left(\frac{\Delta C^*}{k_c S_C}\right)^2 + \left(\frac{\Delta h^*}{k_h S_h}\right)^2 + R_T f(\Delta C^* \Delta h^*)} \tag{6}$$

where the constant values of k_L (lightness), k_C (chroma), and k_h (hue) were considered unity. Further variables involve the hue rotation term (R_T), and the compensation for lightness (S_L), chroma (S_C), and hue (S_h) [34].

The statistical analysis was performed in line with ISO/TS 23031:2020 (E) [35]. The Mean Color Difference from the Mean (MCDM) is calculated to evaluate the color difference between test and reference spectra. To conduct spectrum analysis and compare the spectra of the target surfaces, the Root-Mean-Square Error (RMSE) for each quantitative variable is calculated as below

$$RMSE = \sqrt{\frac{1}{N}\sum_{i=1}^{N}(r_{r,i} - r_{t,i})^2} \tag{7}$$

$$MCDM = \frac{1}{N}\sum_{i=1}^{N}\Delta E(C_i, C_m) \tag{8}$$

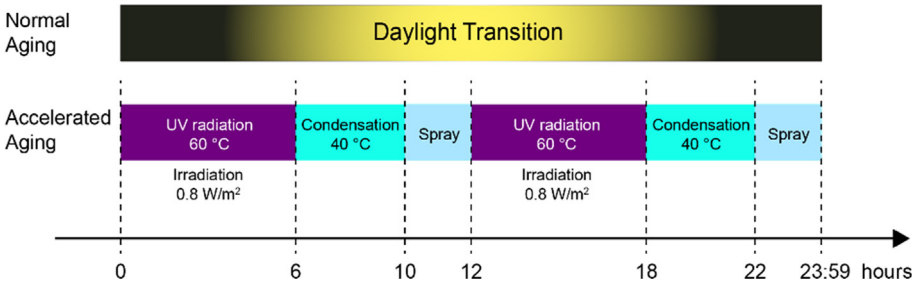

Fig. 2. Aging cycle using a QUV weathering chamber as per ASTM G154.

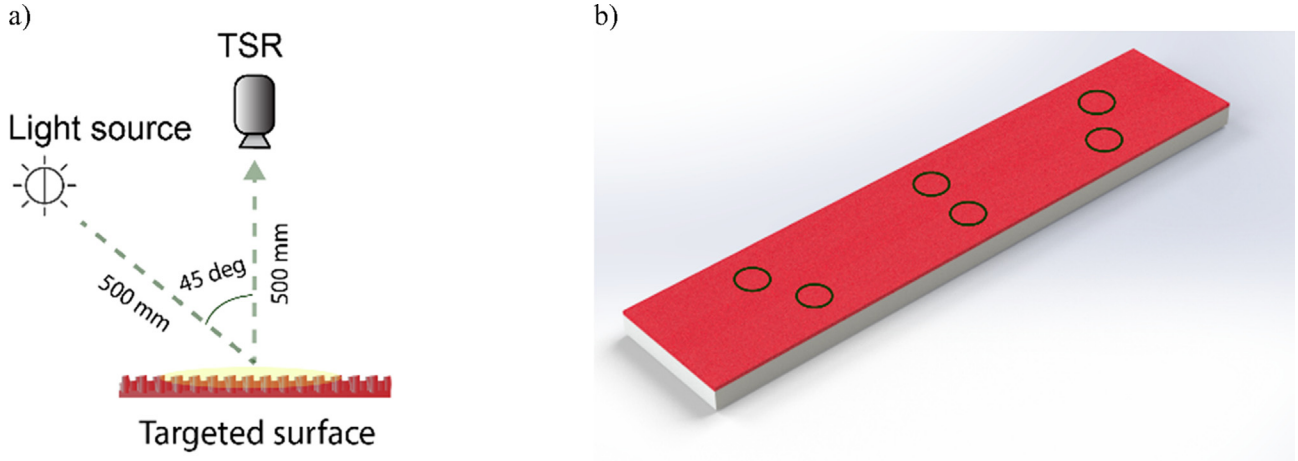

Fig. 3. a) A schematic view of the measurement setup for color appearance, and b) Illustration of appearance measurement locations across each DMA specimen.

where N is the number of reflectance readings, r_t and r_r are the tests and references spectrum, C_i and C_m indicate the colors coordinate of the i^{th} measurements, and the reflectance average, respectively.

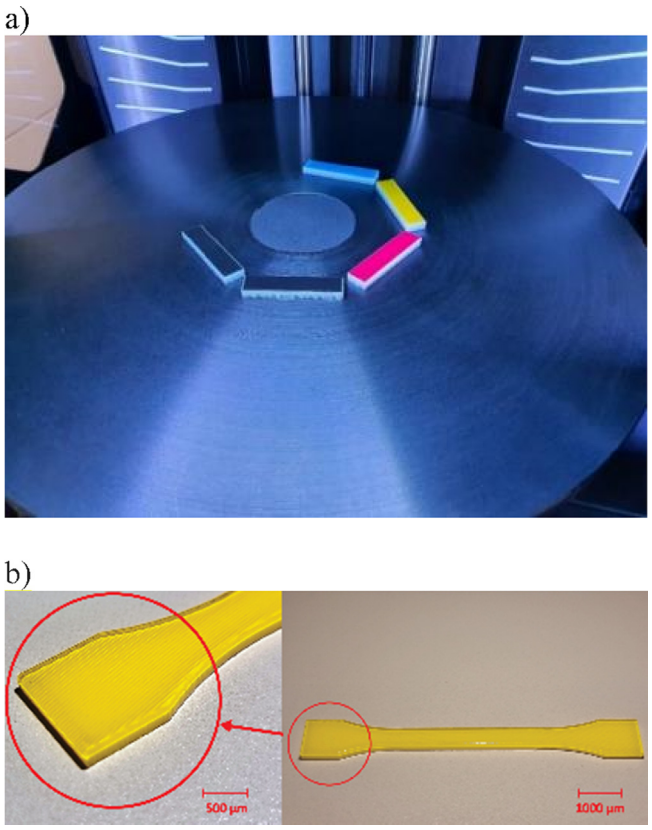

Fig. 4. a) DMA coupons printed in the inner swath, and b) view of un-aged tensile coupons at different scales.

2.4. Physico-mechanical performance characterization

To characterize the extent of degradation in the polymeric 3D-printed coupons after each aging interval, physico-mechanical properties were measured by employing viscoelastic (Dynamic Mechanical Analysis - DMA) and tensile property changes. DMA analysis of polymeric coupons allows for determining the Glass Transition temperature (T_g) and any T_g shift resulting from aging [36]. ASTM D4065 [37] was employed to test the coupons under 3-point bending mode on a Discovery DMA 850 (TA Instruments, USA), with coupon dimensions of 60 × 13 × 3 (mm) (Fig. 4 (a)). Tests were performed at 1 Hz with an amplitude of 20 µm. Temperature ramp tests were conducted at lower degradation temperatures of the material, ranging from 20 °C to 95 °C, at a rate of 2 °C per minute. Two coupons were tested for each batch, and the average T_g was reported. The T_g values were calculated using TRIOS 5 software based on the corresponding temperature of the maximum peak value of the tan δ curve.

The strength value and tensile modulus of the polymer material were determined based on the ISO 527–02 standard [38] as a function of aging duration. Uniaxial tensile testing was performed on dogbone-shaped coupons of 75 × 10 × 2 (mm) (Fig. 4 (b)), using an Instron 5966 (Instron, USA) universal testing machine at a 2 mm/min loading rate. An AVE2 video-extensometer was used to measure mechanical strain.

The tensile chord modulus of bilayer material was determined by force–displacement curves, and ultimate tensile stress was used to report polymer strength. The material response is characterized based on material stiffness (E-Modulus, E) and strength (σ_s) changes. The slope of the stress–strain curve is used to calculate the chord modulus, and the stress–strain curve maximum is represented as the ultimate strength. The retention curves for stiffness and strength are then calculated as follows

$$E\ \ retention = \left(\frac{E_c}{E_r}\right) \tag{9}$$

$$\sigma_s\ \ retention = \left(\frac{\sigma_{sc}}{\sigma_{sr}}\right) \tag{10}$$

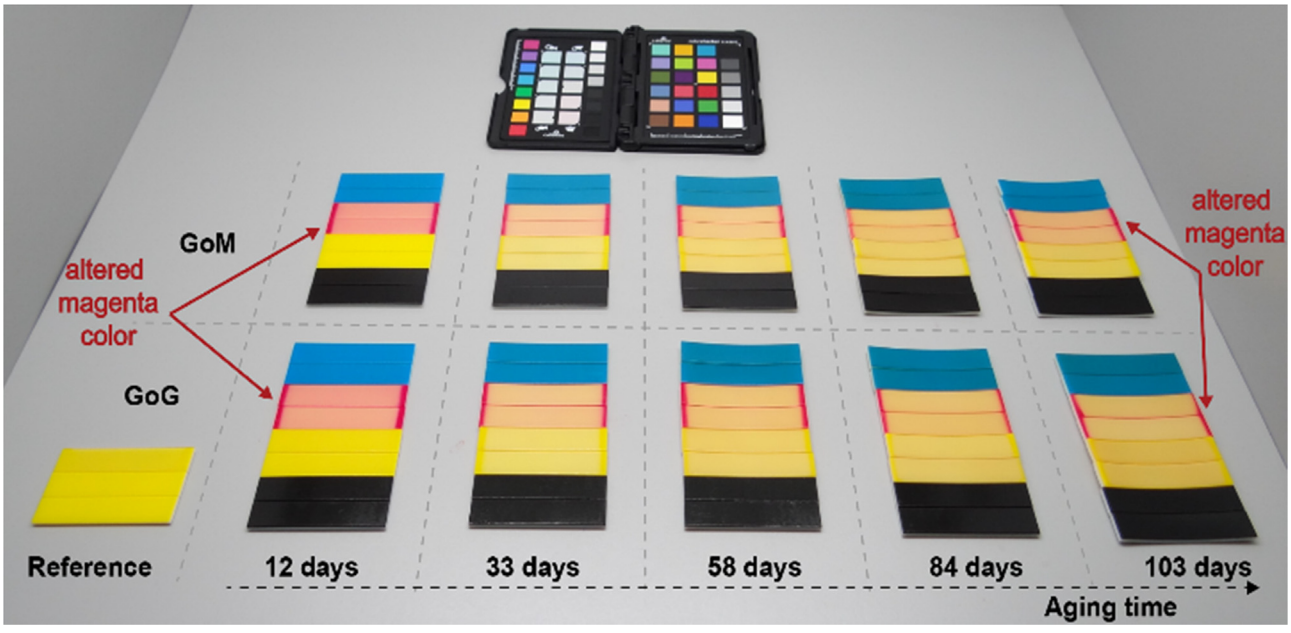

Fig. 5. DMA coupons before and after weathering exposure for different periods, as observed under D50 daylight illumination. Dark-red areas on the margins of magenta represent the original color covered by sample holders. (For interpretation of the references to color in this figure legend, the reader is referred to the web version of this article.)

where E_c and σ_{sc} denote the mean values of E and σ_s for aged coupons, and E_r and σ_{sr} are the mean values for un-aged (as-printed) references. Furthermore, property-retention values have been used to compare elastic modulus and glass transition temperature variation due to accelerated aging. The curvature in the bent coupons, i.e., the distance from the center of the arc and its base (sagitta), was measured using a digital caliper.

2.5. Multivariate analysis

The initial statistical analysis and classification were performed using Detrended Correspondence Analysis (DCA) to select the classification model based on gradient length. The Redundancy Analysis (RDA) is a valid model if the gradient length in the DCA analysis is short (less than3); otherwise, Correspondence Canonical Analysis (CCA) would be more appropriate [39]. Accordingly, because of the short gradient length (less than 0.1), multivariate analysis of the response variables based on the studied parameters was performed using RDA and Spearman rank correlations.

RDA is a multivariate extension of linear regression to matrices containing dependent and independent variables. RDA can also be described as Principal Component Analysis (PCA) with instrumental variables. The model assumes that two datasets have distinct functions [40]. This study included color attributes (dL, dC, and dh) in the matrix of appearance variables. Statistical and Taguchi analyses were performed using Origin 2022 (OriginLab, Northampton, MA, USA), R statistical software 4.2.1 (The R Foundation for Statistical Computing, Vienna, Austria), and Minitab 21 (State College, PA, USA), respectively.

3. Results and discussions

3.1. Color appearance evaluation

Fig. 5 illustrates DMA coupons after aging for the selected periods of time. MCDM results for CIEDE2000 in Fig. 6 (a) present a significant color difference for aged magenta samples compared to their as-printed color. While black parts reflect comparably low

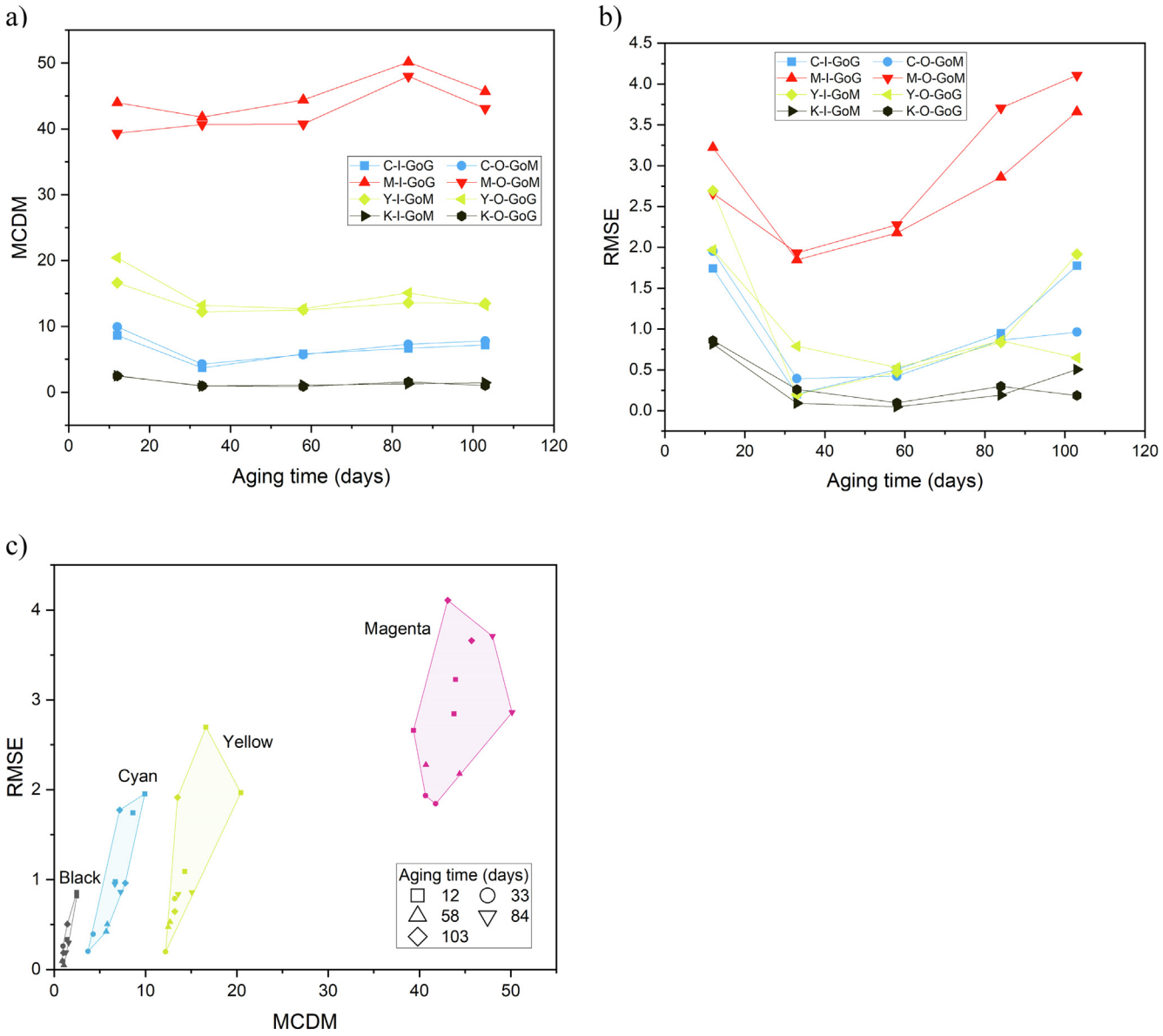

Fig. 6. a) MCDM for CIEDE2000 color difference, b) associated RMSE after the aging process, and c) MCDM vs. RMSE based on a convex hull containing results.

MCDM for different aging periods, cyan and yellow coupons exhibited more noticeable color differences. RMSE follows a similar trend (Fig. 6 (b)), with a strong Spearman rho (rs) correlation observed between MCDM and RMSE with rs = 0.86 and P-value = 1.5E-12. According to the convex hull containing results for each color in Fig. 6 (c), magenta-colored layers exhibited a more significant variation in color appearance because of aging compared to other investigated photo resins, particularly VeroBlackPlus, regardless of the swath and finish used. Nevertheless, a higher color difference was also observed in the GoG coupons compared to their GoM pair.

In general, MCDM and RMSE values were significantly higher at the beginning of aging (after 12 days) compared to 33 days, reached minimum values between 33 and 58 days, and increased again after 84 days (Fig. 6 (a) and (b)). Over time, the variation in lightness, chroma, and hue provides more insight into the alteration of color attributes (Fig. 7 (a)). The hue of cyan and yellow photo resins increased with aging, while it dramatically decreased for magenta samples, with a more dominant effect for GoG finishes. Over more extended periods, however, variations in hue reached a plateau, especially after 84 days. In Fig. 7 (b), magenta samples displayed a significant variation in hue, showing comparable hues as yellow samples at longer aging times. Black samples, however, displayed closer values of u′ and v′, indicating a more negligible hue difference. In supplementary materials available in Appendix A, Figs. A1 and A2 represent the mean values for spectral measurements and detailed CIE1976 u′, v′ chromaticity diagrams for all the studied photo resins.

3.2. Physico-mechanical performance

Fig. 8 illustrates tensile stress–strain curves after testing polymeric MJT coupons from different finishes and aging durations. During the initial days of aging, the tensile response of the material exhibits an increase in the stiffness, strength, and strain-to-failure of the polymeric materials compared to the reference un-aged coupons. A reduction in the mechanical parameters is observed after long-term aging. It can also be observed that the two finishes also indicate remarkably similar behavior in terms of mechanical response.

Fig. 9 (a)-(c) illustrates property-retention plots, for the elastic modulus, strength, and strain-to-failure of polymeric coupons as a function of aging duration for two different finishes. It can be observed that throughout accelerated aging, the elastic modulus retention for both the finishes (Fig. 9 (a)) follows a monotonic increase till 58 days, where the retention values increase above 100%, signifying an improvement in the mechanical properties. During this short-term aging, it can be hypothesized that the combination of temperature and UV exposure can lead to a further post-curing which can be initiated due to photo- and thermal effect [41] inside the polymeric material leading to a higher degree of polymerization, re-arrangement and residual crosslinking of the polymeric chains. This chemical transformation can hence lead to increased resistance towards a uniaxial deformation, which can be manifested as an increase in the stiffness of the material. In the case of the materials strength and strain-to-failure, the speculated post-curing effect was limited to 33 days and 12 days, respectively, whilst the onset of degradation starts at an earlier stage.

The behavioral changes in the material due to aging were observed in the long-term as changes in the mechanical properties by the property-retention plots. An interplay of the crosslinking, thermo photooxidation, chain scission, and crazing of the polymeric chain leads to changes in the structural performance that gradually result in degradation over long-term exposure [42]. In our case, strength, and strain-to-failure reduction due to degradation are observed, whilst stiffness remains practically unaffected at the end of the aging duration, compared to the original state (day 0). It can be hypothesized that the combined effect of temperature, water, and UV may lead to increased surface roughness and cause micro-crack formation. As such, despite the initial post-curing sites

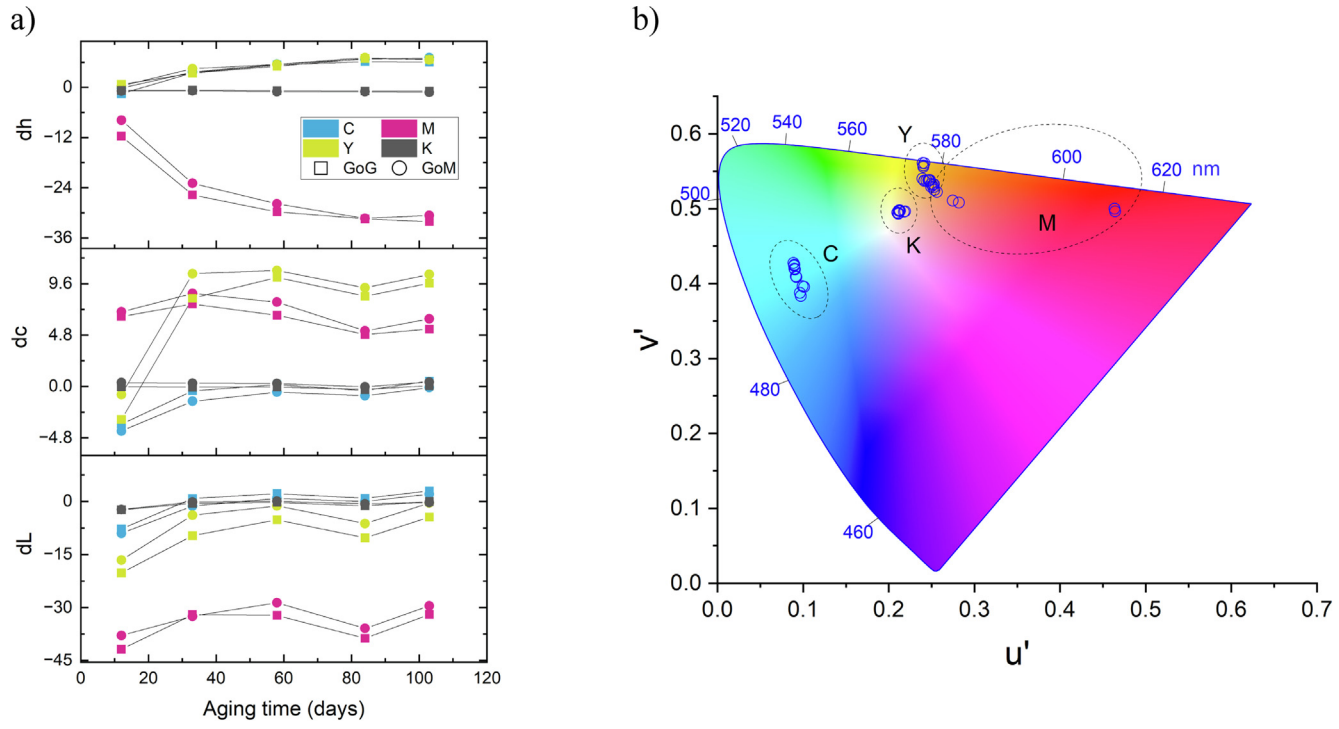

Fig. 7. a) Distribution of variation in the mean value of lightness (l), chroma (c), and hue (h) over aging time, and b) the distribution of the mean hue stimuli in the CIE1976 u′, v′ chromaticity diagram for aged coupons. The blue line indicates the corresponding wavelengths between 420 and 680 nm for each color. (For interpretation of the references to color in this figure legend, the reader is referred to the web version of this article.)

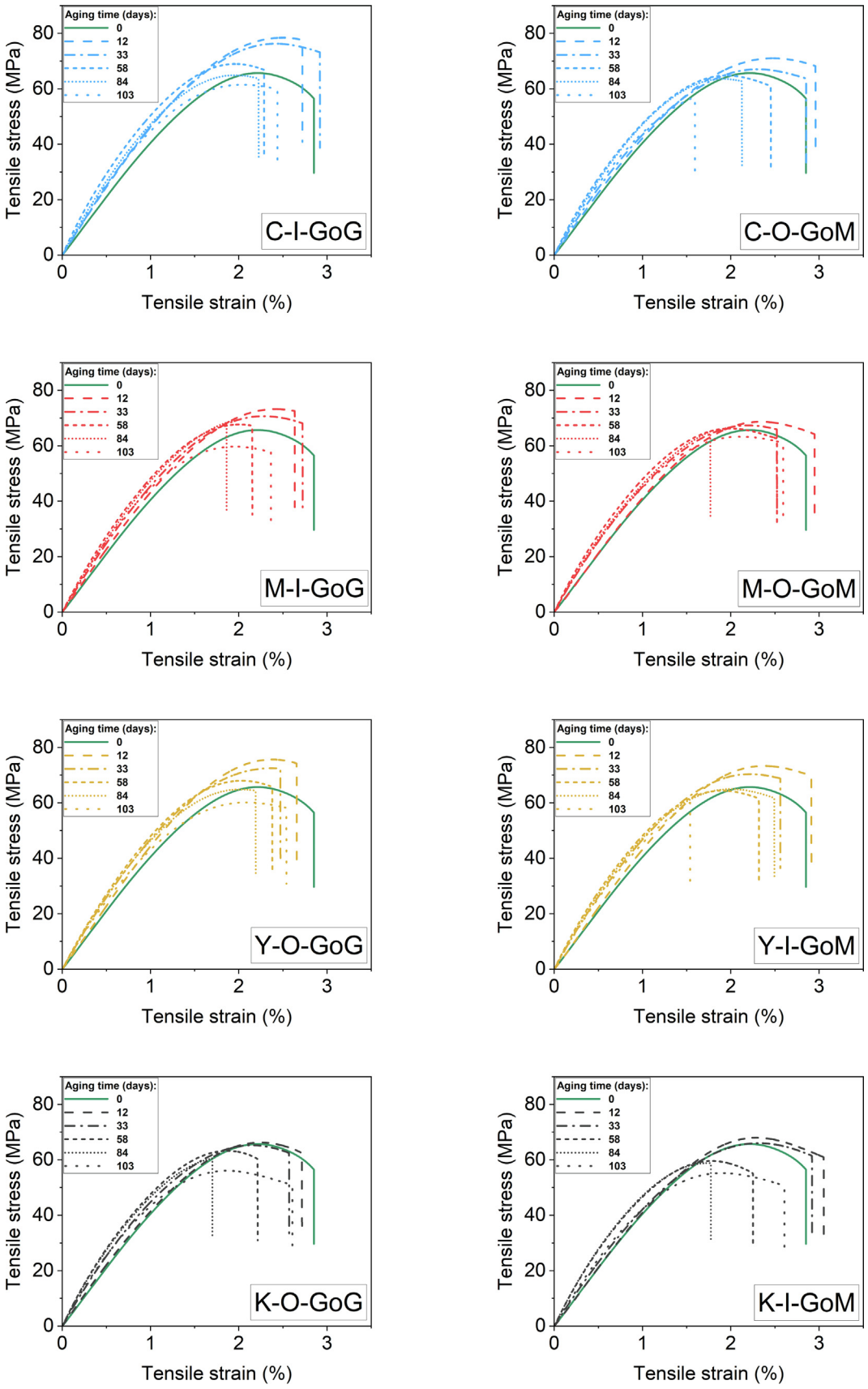

Fig. 8. Stress–strain curves for aged coupons compared to the un-aged reference.

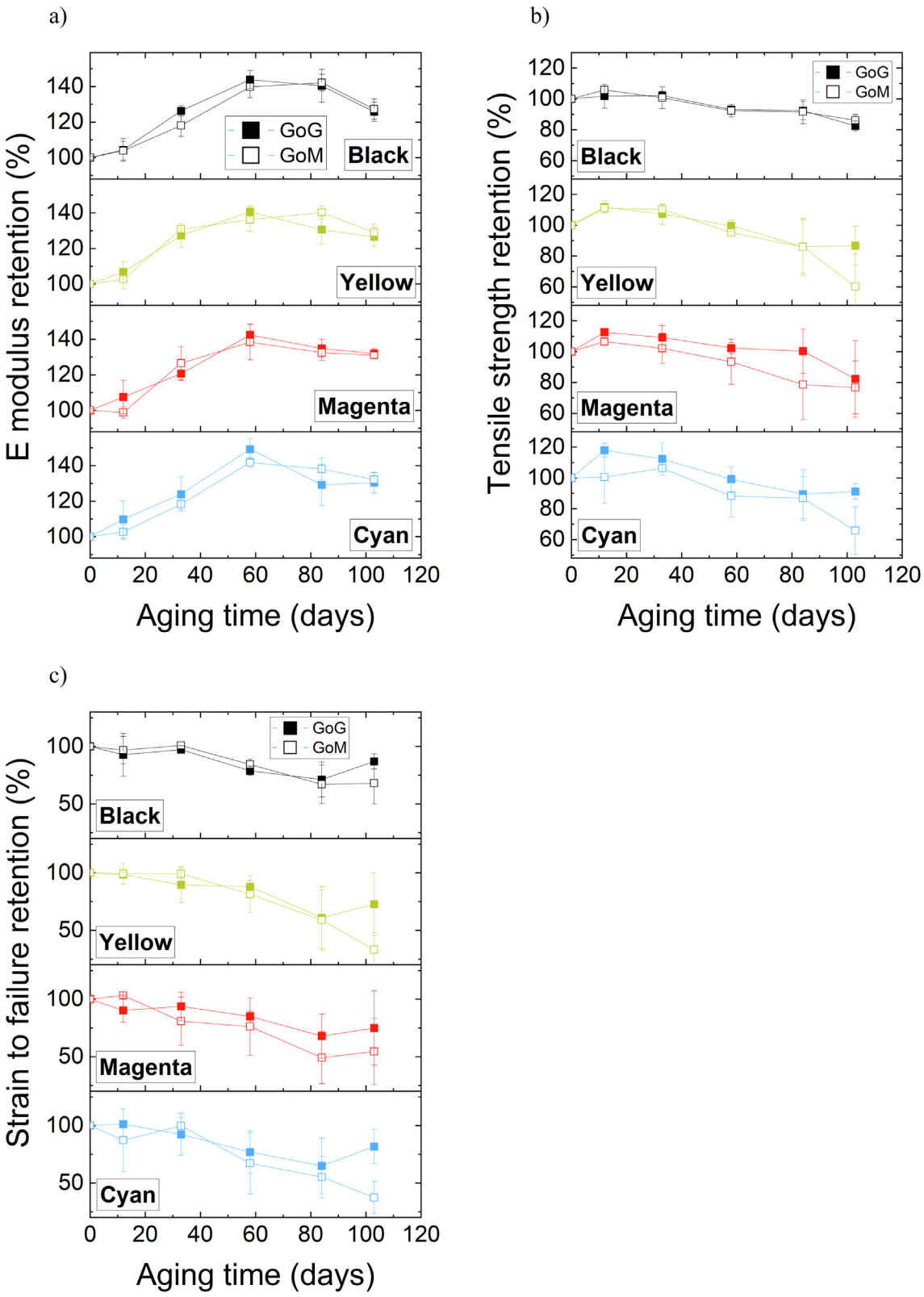

Fig. 9. a) E modulus (stiffness), b) strength, and c) strain-to-failure retention vs. aging time for studied photo resins. Error bars represent Standard Deviation (SD).

for crack initiation may at the same time be generated, thus leading to a reduction in both the strength and strain-to-failure. The post-curing effect leads to brittleness, which causes an increase in stiffness, until day 58. After that, aging degradation is more prominent than post-curing, causing a reduction in stiffness. Although at the end of the aging period, stiffness remains at higher levels than in the original state, it is evident that if aging continues further than 103 days, stiffness will eventually degrade. It is also

Table 3
Stiffness retention for different samples and finishes.

Aging time (Days)	C-I-GoG	C-O-GoM	M-I-GoG	M-O-GoM	Y-I-GoM	Y-O-GoG	K-I-GoM	K-O-GoG
12	109.78	102.65	107.47	98.87	102.71	106.75	103.92	104.32
33	123.95	118.34	120.64	126.54	130.82	127.24	118.04	126.30
58	149.21	141.76	142.45	138.34	136.22	140.53	139.77	143.84
84	129.14	138.09	134.82	132.49	140.18	130.53	142.10	140.35
103	130.37	132.19	131.93	130.94	129.00	126.51	127.29	125.77

Table 4
Strength retention for different samples and finishes.

Aging time (Days)	C-I-GoG	C-O-GoM	M-I-GoG	M-O-GoM	Y-I-GoM	Y-O-GoG	K-I-GoM	K-O-GoG
12	117.99	100.55	112.58	106.53	111.07	111.83	105.82	101.78
33	112.39	106.27	109.24	102.15	110.27	107.22	100.71	102.18
58	99.13	88.24	102.34	93.41	95.23	99.70	92.28	93.14
84	89.56	86.83	100.32	78.60	85.98	86.11	91.65	92.39
103	91.23	65.82	82.27	76.68	60.15	86.78	86.10	82.38

Table 5
Strain-to-failure retention values for different samples and finishes.

Aging time (Days)	C-I-GoG	C-O-GoM	M-I-GoG	M-O-GoM	Y-I-GoM	Y-O-GoG	K-I-GoM	K-O-GoG
12	101.28	87.22	90.27	103.22	99.35	98.46	96.89	92.73
33	92.35	99.80	93.77	80.82	99.20	89.60	100.99	97.27
58	76.95	67.20	85.13	76.20	81.49	87.96	84.39	78.88
84	65.04	55.22	67.94	49.19	58.94	60.87	66.98	71.22
103	81.71	37.36	74.94	54.55	33.09	72.71	68.02	86.92

seen from Fig. 9 that GoG coupons generally maintained higher stiffness, strength, and strain-to-failure than GoM coupons after 103 days of aging.

During the aging, a ductile to brittle behavior transition was observed. The extent of the plastic deformation and softening in the tensile stress–strain curve were reduced in samples aged for a longer duration. It was contrary to un-aged, and samples aged for a shorter duration. Interestingly, the polymeric coupons also showed a gain in the strain to failure and tensile strength at the end of the aging duration (103 days), especially in the GoG finish. This could be attributed to recombination and residual crosslinking activated due to long UV exposure, which could help gain both the tensile strength and correspondingly the strain to failure. Similar observations have been also reported by Woo et al. [43].

Tables 3-5 present the property-retention percentage results for all three mechanical parameters.

To investigate the changes observed in tensile testing further, DMA was used to substantiate the findings viscoelastically. Fig. 10 presents storage modulus (E′) which is a measure of stiffness as a function of temperature (of testing). Compared to the un-aged reference, aged samples exhibited lower stiffness, which does not coincide with the tensile testing results shown in Fig. 8 and Fig. 9 due to a weak baseline for measurement of the stiffness transition. Fig. 11 shows the tan d curves for un-aged and aged DMA coupons. A decrease in the peak value of the tan δ curve indicates a worsening of damping behavior. In contrast, shifts in the peak value indicate intrinsic changes because of aging that may correspond to degradation or improvement in the viscoelastic performance.

Fig. 12 depicts the changes in the absolute value of T_g (°C), calculated from the tan d curve obtained from DMA. The variation in the glass transition temperature exhibited a similar trend when compared with the stiffness retention values. The mean T_g values of the aged polymeric coupons increased significantly until day 58, compared with the reference mean value of 73.3 °C resulting from the as-printed coupons. There was a noticeable increase in the T_g of the studied materials (CMYK) within the first 12 days. T_g values continued to increase to a peak of 83.9 °C at 58 days (114% retention) and then decreased to 79.6 °C at the end of aging (103 days). Both the GoG and GoM finishes, as well as the cyan and magenta colors, followed the same trend. However, the black and yellow coupons reached their maximum peak value after 84 days of aging.

Residual post-curing was noticeable as a potential reason behind the increase in the T_g values due to the combined effect of UV, temperature, and moisture. Post-curing typically causes re-arrangement of the polymeric chains and leads to strengthening [44,45]. The polymeric chain re-arrangement leads to a denser polymeric chain network, creating more deformation resistance [46]. Hence, the stiffness and T_g of the polymeric coupons were significantly increased for 58 days of aging. Fig. 13 concludes the variation in T_g and E from Fig. 9 (a) and Fig. 12. It illustrates T_g and E, occurring after 58 days of aging, a period that post-curing becomes less pronounced than degradation. Supplementary data for mechanical and physical evaluation is available in Appendix B.

Fig. 14 shows coupon deformations over aging regimes, presented as a slight bend. According to the formula for the sagitta of a circular arc, the curvature of the aged coupons d is related to their length l and radius of curvature R_1

$$d = R_1 - \sqrt{R_1^2 - \frac{l^2}{4}} \tag{11}$$

where d is the sagitta, l is the length of the as-printed specimen, and R_1 is the radius of the arc.

As shown in Fig. 15, the curvature of MJT coupons increased over time regardless of their manufacturing condition, reaching a maximum between 84 and 103 days of aging. GoM samples generally showed more curvature for the same color than GoG pairs after aging for extended periods. During printing and post-processing, the only difference between GoG and GoM finishes is retaining a thin layer of support material. As with the color appearance results, black coupons exhibited the lowest sagitta values compared to the Vero photo-resins studied.

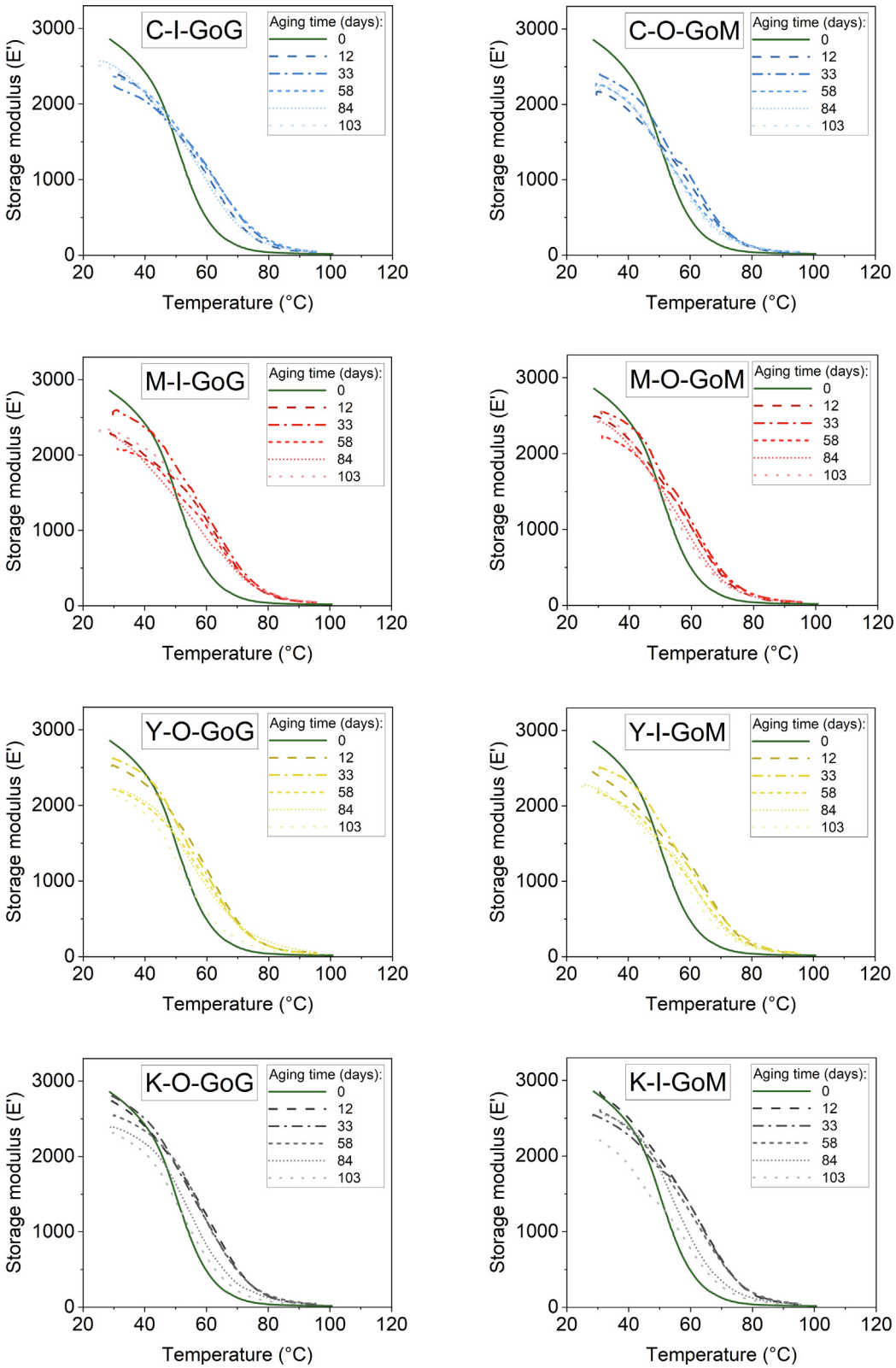

Fig. 10. Storage modulus (E') vs. temperature graphs for aged coupons compared to the un-aged reference (green curves). (For interpretation of the references to color in this figure legend, the reader is referred to the web version of this article.)

3D printing using the J55 printer imposes a semicircular-layered structure due to the centrifugal force generated by rotating the build platform. Further UV absorbance during the aging process may have altered the internal structure of polymeric chains in the layer-by-layer structure, resulting in curvature along the length of DMA coupons. In other words, covalent bonds link mass units, such as monomers to polymer chains, the formation of polymer networks via crosslink polymer chains, and connect polymer

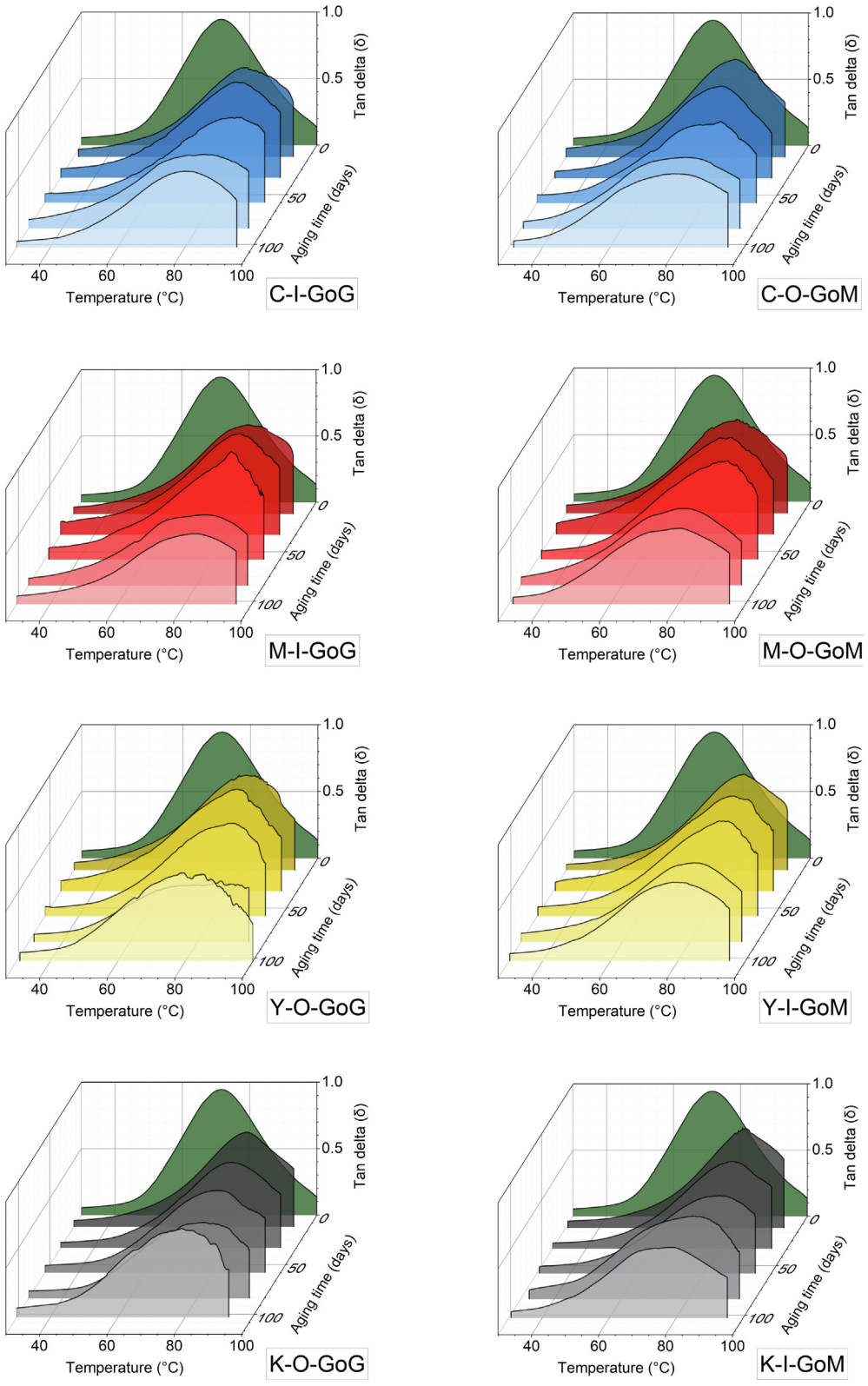

Fig. 11. Damping (Tan δ peak) vs. temperature graphs for aged coupons compared to the un-aged reference (0 days).

networks from distinct layers asymmetrically. This statement is supported by the resulting lower UV absorbance of the dark colors (lower lightness) and GoG finishes compared to GoM due to the retention of a thin layer of support material between white and colored layers.

3.3. Statistical analysis

RDA results are presented in Fig. 16 as ranking diagrams using figurative symbols. The short gradient length in the DCA with axis lengths less than 0.14 for all DCAs confirmed the suitability of RDA

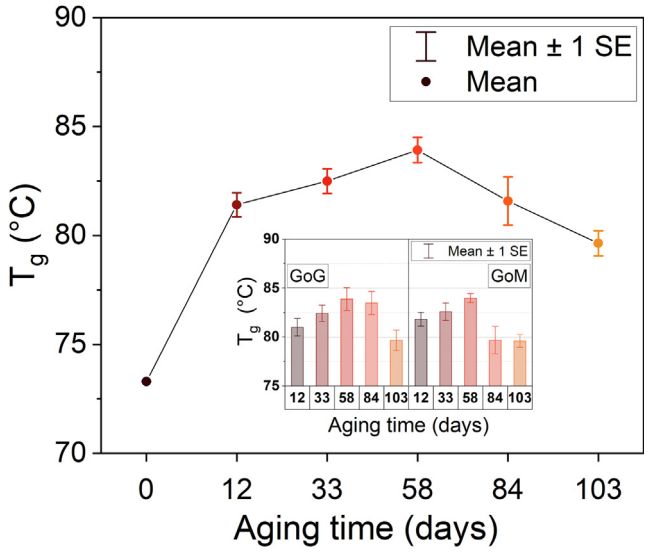

Fig. 12. Arithmetic mean values for T_g and Standard Error (SE) over the aging process.

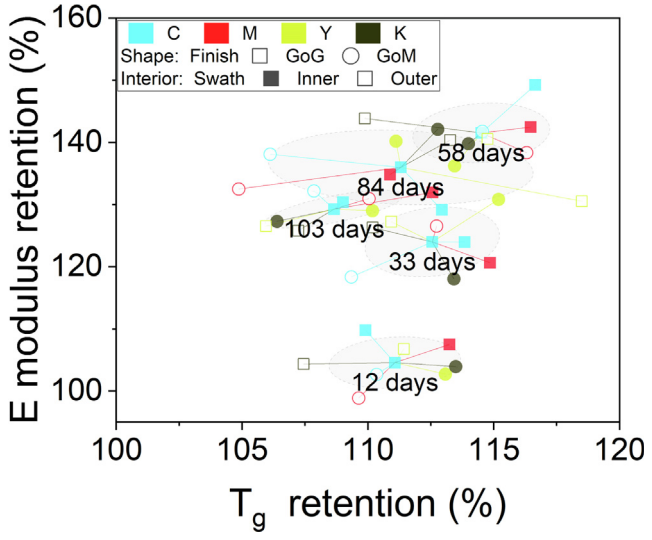

Fig. 13. Variation in elastic modulus vs. glass transition temperature of aged MJT coupons. Each aging period represented 95% confidence centroid ellipses in the gray zone.

results to discuss the link between color attributes and physico-mechanical responses. In Table 6, the first two Principal Components (PCs) account for 95.20% of the variance in the response variables, i.e., strength retention, stiffness retention, and T_g. Therefore, two PCs are appropriate enough to clarify the possible correlation among the data.

The first and second principal components (PC1 and PC2) are indicated by horizontal and vertical axes for related vector colors. Angles between vectors represent corresponding correlations of variables, with a smaller angle indicating a more significant correlation. Positively correlated variables are represented by vectors pointing in the same direction and vice versa. With 58 days of aging, T_g and stiffness retentions were primarily increased, with the highest contribution from PC2 aligned with the increase in dh. Whereas strength was primarily affected by PC1, which tends to sharply increase generally within the first 12 to 33 days of aging due to the increased lightness variation in the color appearance (dL). These results are in agreement with the observation in Fig. 7 (a), Fig. 9, and Fig. 12. However, the variation in chroma (dC) was significantly higher at the end of the aging experiment (103 days) for most of the materials. The opposite direction of vectors for dC and stiffness demonstrated a correlation of rs = -0.45. Nevertheless, the correlation between color difference (MCDM) and mechanical performance during the aging process was weak for all materials except magenta photo resins, as indicated by the different angles between the color attribute vectors.

3.4. Taguchi analysis

In Fig. 17, the main effect plots for data mean at different aging times illustrate that color solely had the most considerable effect on color difference and RMSE, with the highest significant effect in magenta samples, followed by yellow and cyan. Compared to other photo resins, black samples showed a negligible response. While the swath and finish input variables did not significantly affect MCDM output, the GoM finish contributed to a slightly higher RMSE. The selection of swaths in the inner region did not reduce RMSE at the beginning and end of the aging period. It did not significantly affect the color appearance over time.

In terms of the physico-mechanical response to the variables studied (Fig. 18), the trend was not as straightforward as color appearance. In contrast to yellow samples, which showed the highest E modulus after 33 days of aging, black and cyan samples demonstrated the highest E modulus after 58 days of aging. Generally, the highest T_g values were observed for magenta and yellow hues among the studied photo resins, with similar trends observed

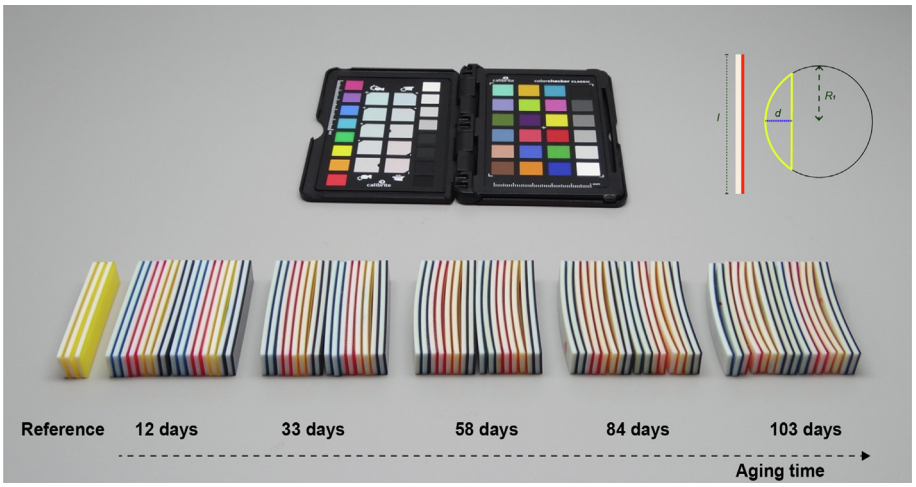

Fig. 14. Side view of DMA samples representing the bending in pieces over 103 days of aging time as observed under D50 daylight illumination.

in color appearance analyses. However, a direct link between mechanical response and color was not observed. This is because colors on the MJT objects changed over time, and the response to environmental aging was altered as a result. A greater UV absorbance of magenta materials compared to cyan specimens during the aging test may clarify the post-curing effect, leading to more rigid polymers with altered colors and mechanical properties.

Based on the finishing options, matte finishes between layers during the first 58 days led to lower E modulus and higher T_g. After 84 days, however, the response changed. In terms of swath selection on the build tray, 3D printing in the inner area of the rotary disc resulted in higher values of E and T_g. The results suggest that swath selection impacted mechanical performance despite its negligible importance in terms of color appearance. The signal-to-noise ratio plots in Appendix C confirm the same trends.

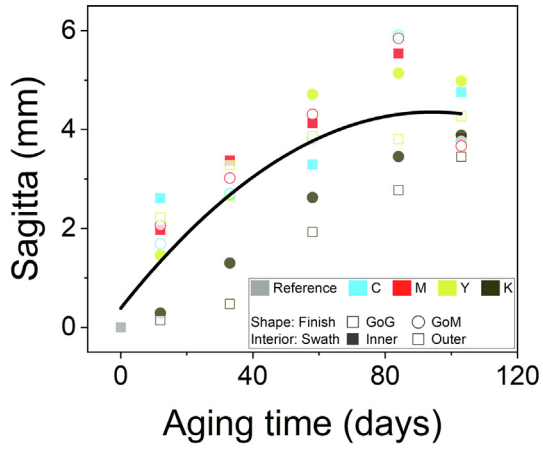

Fig. 15. Results of fitting the mean values for sagitta concerning the curvature appearing over the aging process (R^2: 0.63).

4. Conclusions

In this work, a PolyJet 3D printer has been employed to manufacture bilayer polymer structures on a rotary build platform based on Material Jetting technology. Our study focused on the appearance and physico-mechanical properties of acrylic-simulated parts over 103 days of accelerated aging. Taguchi analysis was used to determine the impact of processing characteristics, such as color, position on the build platform (swath), and finishing options between layers on the response variables. A desirability analysis was set to minimize the color and corresponding RMSE values and maximize the elastic modulus and glass transition temperature. This study led to the following conclusions:

1. Studied polymer coupons exhibited an increase in tensile and viscoelastic performance. The stiffness and strength of the materials increased after 12 days of aging, with stiffness values continuing to increase until 58 days and strength values diminishing monotonically until the end of the aging duration. On the other hand, strain-to-failure values generally diminished during the aging period.

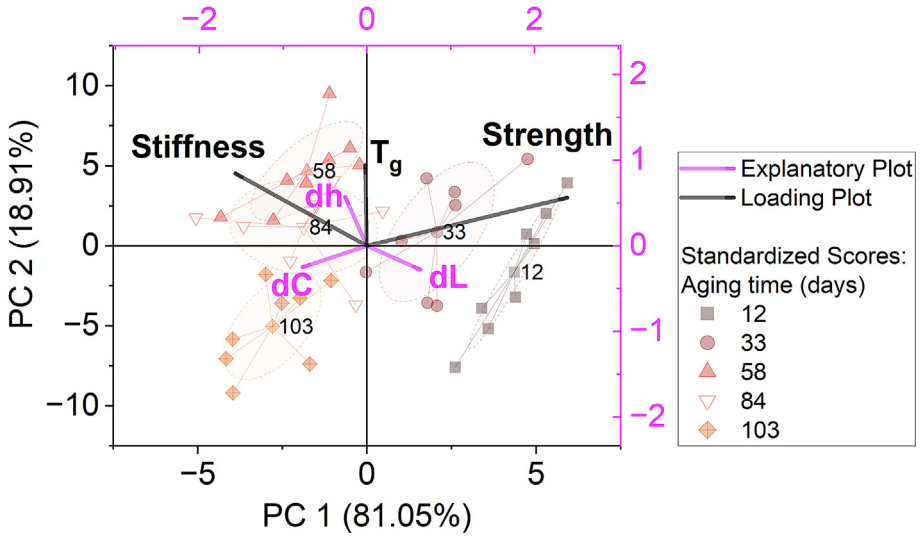

Fig. 16. RDA ordination diagram (triplot) showing aged coupons by denoted points for different aging days, explanatory variables (color attributes; purple vectors), and response variables (mechanical performance - retention; black vectors). Each aging period represented 95% confidence centroid ellipses in the gray zone. (For interpretation of the references to color in this figure legend, the reader is referred to the web version of this article.)

Table 6
Principal components ranking according to their cumulative roles in PCA.

	Eigenvalues for constrained axe: Explanatory variables			Eigenvalues for unconstrained axe: Principal components		
Ranking	Eigenvalue	Percentage of Inertia (%)	Cumulative Inertia (%)	Eigenvalue	Percentage of Inertia (%)	Cumulative Inertia (%)
1	14.72	11.65	11.65	63.92	50.56	64.93
2	3.43	2.72	14.36	38.26	30.27	95.20
3	0.01	0.01	14.37	6.06	4.80	100.00

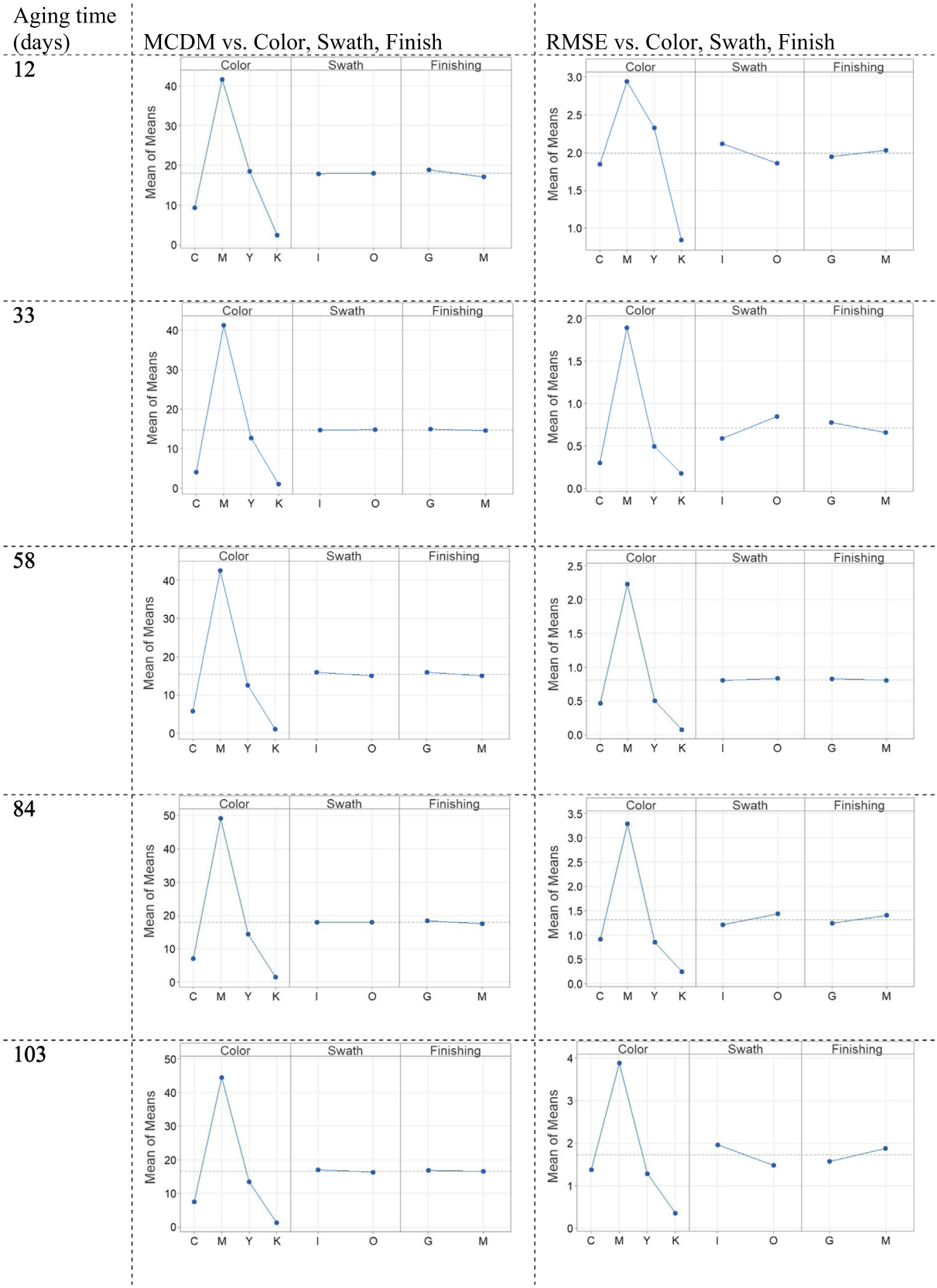

Fig. 17. Main effects plots for data means according to Taguchi analysis for the color appearance factors at the different aging times.

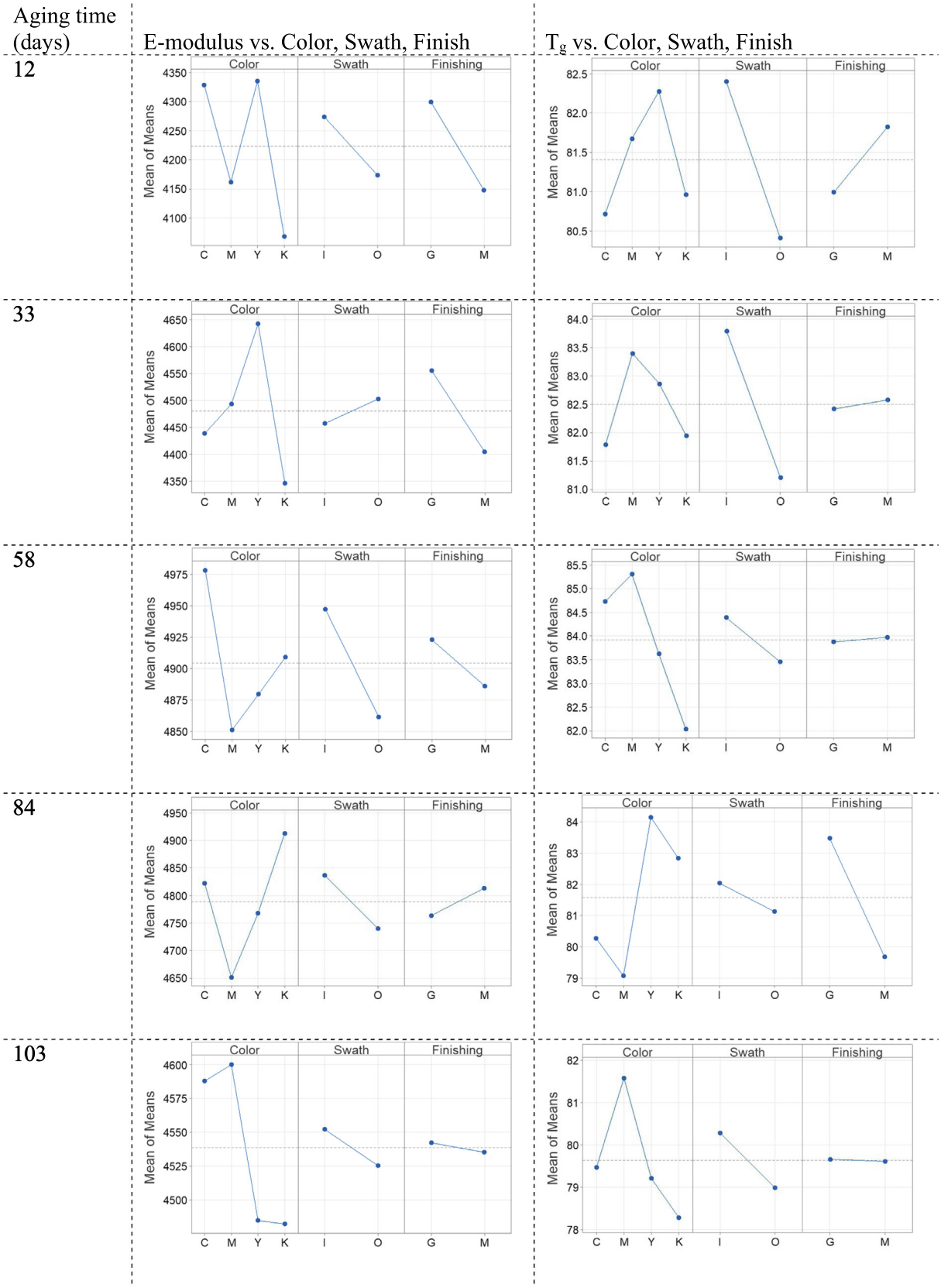

Fig. 18. Main effects plots for data means according to Taguchi analysis for the mechanical performance factors at the different aging times.

2. Based on mechanical performance, cyan photo resin had a higher level of tensile test results over an extended time, and the performance of the Glossy-on-Glossy finish was higher than that of Glossy-on-Matte specimens.
3. As a result of the dynamic response of the photo resins to weathering, distinct colors, and physico-mechanical performance was observed over time. The maximum variation in stiffness and T_g was observed following 58 days of accelerated aging in the QUV chamber. As MJT coupons aged, their curvature, hue variation, and measurement errors for color and stiffness increased, regardless of their manufacturing PPP, reaching a maximum between 84 and 103 days, respectively.
4. Color appearance is solely affected by the photo resin color factor compared to other PPPs studied, while E and T_g were influenced by all the studied PPPs, including color, swath, and finishing. Magenta specimens resulted in a hue distribution remarkably close to yellow materials in the CIE1976 u′, v′ chromaticity diagram after 12 days of aging. For both the color difference and its RMSE, most of the minimum values were reached between 33 and 58 days of the experiment. Black and cyan showed significantly less color difference and higher reliability than magenta and yellow photo resins over different aging periods.
5. Post-curing and the circular layer-by-layer structure observed in MJT coupons were the leading causes for the curvature along the length of DMA coupons. Due to the radial form of layers in 3D-printed coupons, the curvature is propagated into colored layers by forming new covalent bonds in polymer chains.
6. Multivariate RDA analysis revealed within the first 12 to 33 days of aging, lightness variations in the color appearance (dL) were involved as the first principal components (PC1). After 58 days of aging, T_g and stiffness retentions were primarily increased, with the highest contribution coming from PC2, which aligned with the increase in dh. At the end of the aging experiment (103 days), most materials showed a significantly higher variation in chroma (dC). Furthermore, a strong negative correlation was observed between dC and stiffness. It is proposed that the correlation is a consequence of the different responses of coupons with various appearances to UV absorbance, which significantly impacts the material properties.
7. According to the Taguchi analysis, color appearance is solely affected by the photo resin color factor compared to other PPPs studied. However, E and T_g were influenced by all the studied PPPs, including color, swath, and finishing. As a result of printing on the outer swath or selecting a Glossy-on-Matte finish, the MJT coupons appear to have less variation in elastic modulus and glass transition temperature. In terms of color, fidelity based on mean CIEDE2000 color differences, black and cyan showed significantly less color difference and higher reliability than magenta and yellow photo resins over different aging periods.

In summary, this study demonstrated the importance of understanding the mechanisms that affect the appearance and performance of multi-layered 3D-printed objects from the long-term perspective. Future research will have the opportunity to examine how different aging conditions, processing parameters, and materials and compositions affect the long-term properties of printed materials, intending to improve the durability and longevity of 3D-printed objects. It opens new avenues for improving 3D printing algorithms and multi-layer compatibility in additive manufacturing.

Data availability

The main part of the raw/processed data required to reproduce these findings is available at https://doi.org/10.5281/zenodo.7314465.

The rest cannot be shared at this time as the data also forms part of an ongoing study.

CRediT authorship contribution statement

Ali Payami Golhin: Conceptualization, Methodology, Investigation, Data curation, Formal analysis, Visualization, Writing – original draft, Writing – review & editing. **Chaman Srivastava:** Conceptualization, Methodology, Data curation, Writing – review & editing. **Are Strandlie:** Writing – review & editing, Supervision, Project administration, Funding acquisition. **Aditya Suneel Sole:** Writing – review & editing, Supervision. **Sotirios Grammatikos:** Writing – review & editing, Conceptualization, Supervision, Funding acquisition.

Data availability

https://doi.org/10.5281/zenodo.7314465

Declaration of Competing Interest

The authors declare the following financial interests/personal relationships which may be considered as potential competing interests: Ali Payami Golhin reports financial support, and article publishing charges were provided by Horizon 2020 (EU) ApPEARS-ITN project [grant No. 814158]. Ali Payami Golhin reports financial support, and travel was provided by the Research Council of Norway - LIFETIME project [Ref: 309943].

Acknowledgments

This work was supported by the ApPEARS-ITN project funded by the European Union's H2020 research and innovation program under the Marie Skłodowska-Curie grant agreement No. 814158 and from the LIFETIME project, Ref: 309943, funded by the Research Council of Norway.

Appendix A. Supplementary data

Supplementary data to this article can be found online at https://doi.org/10.1016/j.matdes.2023.111863.

References

[1] J. Yuan, G. Chen, H. Li, H. Prautzsch, K. Xiao, Accurate and Computational: A review of color reproduction in Full-color 3D printing, Mater. Des. 209 (2021) 1–17, https://doi.org/10.1016/j.matdes.2021.109943.
[2] A. Payami Golhin, A. Strandlie, P. John Green, The influence of wedge angle, feedstock color, and infill density on the color difference of FDM objects, J. Imaging Sci. Technol. 65 (5) (2021) 1–15, https://doi.org/10.2352/J.ImagingSci.Technol.2021.65.5.050408.
[3] X. Wei, N. Zou, L. Zeng, Z. Pei, PolyJet 3D Printing: Predicting Color by Multilayer Perceptron Neural Network, Annals of 3D, Printed Medicine 5 (2022) 1–7, https://doi.org/10.1016/j.stlm.2022.100049.
[4] A.P. Golhin, A.S. Sole, A. Strandlie, Color appearance in rotational material jetting, Int. J. Adv. Manuf. Technol. 124 (3) (2023) 1183–1198, https://doi.org/10.1007/s00170-022-10536-1.
[5] G. Elber, M.-S. Kim, Synthesis of 3D jigsaw puzzles over freeform 2-manifolds, Comput Graphics (Pergamon) 102 (2022) 339–348.
[6] R. Chand, V.S. Sharma, R. Trehan, M.K. Gupta, M. Sarikaya, Investigating the dimensional accuracy and surface roughness for 3D printed parts using a multi-jet printer, J. Mater. Eng. Perform. 32 (3) (2023) 1145–1159.
[7] A. Payami Golhin, Generation of micro-and nano-textured surfaces, European Commission, Brussels, 2021, pp. 1-6. https://doi.org/10.5281/zenodo.7293168.
[8] L. Bass, N.A. Meisel, C.B. Williams, Exploring variability of orientation and aging effects in material properties of multi-material jetting parts, Rapid Prototyping J. 22 (5) (2016) 826–834, https://doi.org/10.1108/RPJ-11-2015-0169.
[9] I.Q. Vu, L.B. Bass, C.B. Williams, D.A. Dillard, Characterizing the effect of print orientation on interface integrity of multi-material jetting additive manufacturing, Addit. Manuf. 22 (2018) 447–461, https://doi.org/10.1016/j.addma.2018.05.036.

[10] M. Siegfarth, T.P. Pusch, A. Pfeil, P. Renaud, J. Stallkamp, Multi-material 3D printed hydraulic actuator for medical robots, Rapid Prototyping J. 26 (6) (2020) 1019–1026.
[11] T. Puttonen, M. Salmi, J. Partanen, Mechanical properties and fracture characterization of additive manufacturing polyamide 12 after accelerated weathering, Polym. Test 104 (2021) 107376.
[12] S.A. Grammatikos, M. Evernden, J. Mitchels, B. Zafari, J.T. Mottram, G.C. Papanicolaou, On the response to hygrothermal aging of pultruded FRPs used in the civil engineering sector, Mater. Des. 96 (2016) 283–295, https://doi.org/10.1016/j.matdes.2016.02.026.
[13] S. Kumar, I. Singh, D. Kumar, M.Y. Yahya, S.S. Rahimian Koloor, Mechanical and Morphological Characterizations of Laminated Object Manufactured 3D Printed Biodegradable Poly (lactic) acid with Various Physical Configurations, J. Marine Sci. Eng. 10 (12) (2022) 1954, https://doi.org/10.3390/jmse10121954.
[14] A. Payami Golhin, C. Srivastava, J.F. Tingstad, A.S. Sole, A. Strandlie, S. Grammatikos, Additive manufacturing of multilayered polymer composites: Durability assessment, Proceedings of the 20th European Conference on Composite Materials-Composites Meet Sustainability (Vol 1-6), EPFL Lausanne, Composite Construction Laboratory Switzerland, 2022. https://doi.org/10.5075/epfl-298799_978-2-9701614-0-0.
[15] C. Camposeco-Negrete, Optimization of FDM parameters for improving part quality, productivity and sustainability of the process using Taguchi methodology and desirability approach, Prog. Addit. Manuf. 5 (1) (2020) 59–65.
[16] Y. Duan, L. Zhang, J. Qiao, Y.-J. Wang, Y. Yang, T. Wada, H. Kato, J. Pelletier, E. Pineda, D. Crespo, Intrinsic Correlation between the Fraction of Liquidlike Zones and the β Relaxation in High-Entropy Metallic Glasses, Phys Rev Lett 129 (17) (2022), https://doi.org/10.1103/PhysRevLett.129.175501 175501.
[17] A. Foerster, V. Annarasa, A. Terry, R. Wildman, R. Hague, D. Irvine, D.S.A. De Focatiis, C. Tuck, UV-curable silicone materials with tuneable mechanical properties for 3D printing, Mater. Des. 205 (2021) 109681.
[18] S. Baharnezhad, A. Golhin, In-situ measurement and finite element simulation of thermo-mechanical properties of AA 6063 aluminum alloy for MIG weldment, Mater. Phys. Mech. 32 (2) (2017), https://doi.org/10.18720/MPM.3222017_15.
[19] S. Kumar, I. Singh, S.R. Koloor, D. Kumar, M. Yahya, On Laminated Object Manufactured FDM-Printed ABS/TPU Multimaterial Specimens: An Insight into Mechanical and Morphological Characteristics, Polymers 14 (19) (2022) 4066.
[20] S. Garzon-Hernandez, D. Garcia-Gonzalez, A. Jérusalem, A. Arias, Design of FDM 3D printed polymers: An experimental-modelling methodology for the prediction of mechanical properties, Mater. Des. 188 (2020) 108414.
[21] I. Singh, S. Kumar, S.R. Koloor, D. Kumar, M. Yahya, J. Mago, On Comparison of Heat Treated and Non-Heat-Treated LOM Manufactured Sample for Poly (lactic) acid: Mechanical and Morphological View Point, Polymers 14 (23) (2022) 5098.
[22] N. Vidakis, M. Petousis, N. Michailidis, J.D. Kechagias, N. Mountakis, A. Argyros, O. Boura, S. Grammatikos, High-performance medical-grade resin radically reinforced with cellulose nanofibers for 3D printing, J. Mech. Behav. Biomed. Mater. 134 (2022), https://doi.org/10.1016/j.jmbbm.2022.105408 105408.
[23] Z. Meng, J. He, Z. Cai, F. Wang, J. Zhang, L. Wang, R. Ling, D. Li, Design and additive manufacturing of flexible polycaprolactone scaffolds with highly-tunable mechanical properties for soft tissue engineering, Mater. Des. 189 (2020) 108508.
[24] R.D. Goodridge, R.J.M. Hague, C.J. Tuck, Effect of long-term ageing on the tensile properties of a polyamide 12 laser sintering material, Polym. Test 29 (4) (2010) 483–493, https://doi.org/10.1016/j.polymertesting.2010.02.009.
[25] R. Sepe, S. Franchitti, R. Borrelli, F. Di Caprio, E. Armentani, F. Caputo, Correlation between real geometry and tensile mechanical behaviour for Ti6Al4V electron beam melted thin specimens, Theor. Appl. Fract. Mech. 107 (2020) 102519.
[26] C. Chen, F. Chen, Y. Yang, H. Zhang, Study on appearance and mechanical behavior of additively manufacturing of Ti–6Al–4V alloy by using cold metal transfer, CIRP J. Manuf. Sci. Technol. 35 (2021) 250–258, https://doi.org/10.1016/j.cirpj.2021.06.017.
[27] Y.L. Tee, C. Peng, P. Pille, M. Leary, P. Tran, PolyJet 3D printing of composite materials: experimental and modelling approach, JOM 72 (3) (2020) 1105–1117, https://doi.org/10.1007/s11837-020-04014-w.
[28] Stratasys, Vero: Realistic, Multi-Color Prototypes in Less Time, Stratasys Datasheet, 2022, pp. 1-4.
[29] Stratasys, 3D Printing with Pantone Colors, Stratasys Ltd., 2021, pp. 1-6.
[30] ASTM, Standard practice for operating fluorescent ultraviolet (UV) lamp apparatus for exposure of nonmetallic materials, ASTM G154 (2016) 1-12.
[31] C.I.d. l'Éclairage, Colorimetry CIE 015:2004, Commission Internationale de l'Éclairage, 2004, pp. 1-82.
[32] S. Westland, C. Ripamonti, V. Cheung (Eds.), Computational Colour Science using MATLAB®, Wiley, 2012.
[33] A. International, Standard Practice for Computing the Colors of Objects by Using the CIE System, 2018, p. 45.
[34] G. Sharma, W. Wu, E.N. Dalal, The CIEDE2000 color-difference formula: Implementation notes, supplementary test data, and mathematical observations, Color Res. Appl. 30 (1) (2005) 21–30, https://doi.org/10.1002/col.20070.
[35] Assessment and validation of the performance of spectrocolorimeters and spectrodensitometers, ISO/TS 23031:2020; Graphic technology, International Organization for Standardization: Geneva, Switzerland, 2020.
[36] S.C. Das, D. Paul, S.A. Grammatikos, M.A.B. Siddiquee, S. Papatzani, P. Koralli, J. M.M. Islam, M.A. Khan, S.M. Shauddin, R.A. Khan, N. Vidakis, M. Petousis, Effect of stacking sequence on the performance of hybrid natural/synthetic fiber reinforced polymer composite laminates, Compos. Struct. 276 (2021) 114525.
[37] A.S. D–01, Standard practice for plastics: dynamic mechanical properties: determination and report of procedures, ASTM International West Conshohocken, PA, 2000.
[38] Plastics - Determination of Tensile Properties: Test Conditions for Moulding and Extrusion Plastics, ISO 527-2:2012; ISO/TC 61/SC 2 Mechanical behavior, International Organization for Standardization: Geneva, Switzerland, 2012.
[39] J. Lepš, P. Šmilauer (Eds.), Multivariate Analysis of Ecological Data using CANOCO, Cambridge University Press, 2003.
[40] C.R. Rao, The use and interpretation of principal component analysis in applied research, Sankhyā: Indian J. Statist. Ser. A (1964) 329–358.
[41] F. Segovia, C. Ferrer, M.D. Salvador, V. Amigo, Influence of processing variables on mechanical characteristics of sunlight aged polyester–glass fibre composites, Polym Degradation Stab 71 (1) (2000) 179–184, https://doi.org/10.1016/S0141-3910(00)00168-3.
[42] E. Boinard, R.A. Pethrick, J. Dalzel-Job, C.J. Macfarlane, Influence of resin chemistry on water uptake and environmental ageing in glass fibre reinforced composites-polyester and vinyl ester laminates, J Mater Sci 35 (8) (2000) 1931–1937, https://doi.org/10.1023/A:1004766418966.
[43] R.S.C. Woo, H. Zhu, C.K.Y. Leung, J.-K. Kim, Environmental degradation of epoxy-organoclay nanocomposites due to UV exposure: Part II residual mechanical properties, Compos. Sci. Technol. 68 (9) (2008) 2149–2155, https://doi.org/10.1016/j.compscitech.2008.03.020.
[44] S. Mora, N.M. Pugno, D. Misseroni, 3D printed architected lattice structures by material jetting, Mater. Today 59 (2022) 107–132.
[45] K. Kardel, A. Khoshkhoo, A.L. Carrano, Design guidelines to mitigate distortion in material jetting specimens, Rapid Prototyping J. 27 (6) (2021) 1148–1160, https://doi.org/10.1108/RPJ-08-2020-0192.
[46] Z. Tang, J. Gong, P. Cao, L. Tao, X. Pei, T. Wang, Y. Zhang, Q. Wang, J. Zhang, 3D printing of a versatile applicability shape memory polymer with high strength and high transition temperature, Chem. Eng. J. 431 (2022) 134211.